FULL PAPER

Zr-MOF-808 as Catalyst for Amide Esterification

Beatriz Villoria-del-Álamo,[a] Sergio Rojas-Buzo,[a] Pilar García-García*[a,b] and Avelino Corma*[a]

[a]   B. Villoria-del-Álamo, Dr. S. Rojas-Buzo, Dr. P. García-García, Prof. Dr. A. Corma
        Instituto de Tecnología Química, UPV-CSIC, Universitat Politècnica de València-Consejo Superior de Investigaciones Científicas
        Avenida de los Naranjos s/n 46022 Valencia, Spain
        E-mail: acorma@itq.upv.es
[b]   Dr. P. García-García.
        Present address: Departamento de Ciencias Farmacéuticas, Facultad de Farmacia, CIETUS, IBSAL
        Campus Miguel de Unamuno, University of Salamanca, 37007, Spain
        E-mail: pigaga@usal.es

        Supporting information for this article is given via a link at the end of the document.

Abstract: In this work, zirconium-based metal-organic framework Zr-MOF-808-P has been found to be an efficient and versatile catalyst for amide esterification. Comparing with previously reported homogeneous and heterogeneous catalysts, Zr-MOF-808-P can promote the reaction for a wide range of primary, secondary and tertiary amides with n-butanol as nucleophilic agent. Different alcohols have been employed in amide esterification with quantitative yields. Moreover, the catalyst acts as a heterogeneous catalyst and could be reused for at least five consecutive cycles. The amide esterification mechanism has been studied on the Zr-MOF-808 at molecular level by *in situ* FT-IR spectroscopic technique and kinetic study.

Introduction

Amide is one of the most robust groups[1] present in nature (in proteins,[2] drugs[3] and other synthetic products[4]). Under physiological conditions (neutral pH and room temperature), the amide bond half-life is around 350-600 years.[5,6,7] Due to the extreme inertness associated with their resonance stabilization, the amide bond cleavage has been studied extensively in the last decades,[8,9,10,11,12,13,14,15] and amide esterification with alcohols is a versatile strategy to convert amides into useful synthetic building blocks. Examples of this are picolinic acid or niacin derivate aromatic ester, which are active for apoptosis of human leukaemia cells and rubefacients prodrugs, respectively.[16,17] In nature, protease enzymes can perform peptide bond hydrolysis in proteins through an ATP-dependent process. Inspired by the confined space and active sites of these enzymes (based on transition metals), inorganic artificial systems have been synthesized.[18,19] However, the methodologies employed for the amide esterification require severe conditions, high metal-loading and, in some cases, produce low yields of the desired product due to the low reactivity of the amides (poor electrophiles), the reduced nucleophilicity of the alcohols and the higher thermodynamic stability of the substrates compared to the products.

Different strategies for the esterification of specific activated amides (twisted or distorted) have been postulated using homogeneous catalysts.[20,21] Functionalized secondary or tertiary amides, such as *N*-acyl-*tert*-butyl-carbamates, *N*-acyl-tosylamides or di-*tert*-butyl- *N*-acylimidocarbonates, are

converted into esters using fluoride as catalyst (**Scheme 1**).[22] This halide is a strong nucleophile, which interacts with the amide carbonyl group to generate an acyl fluoride intermediate. The last one is more reactive than the amide group, allowing the nucleophilic attack of alcohol to the carbonyl group.
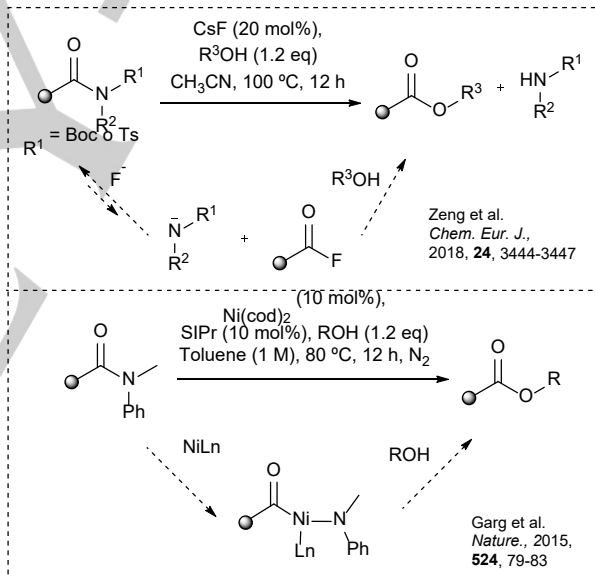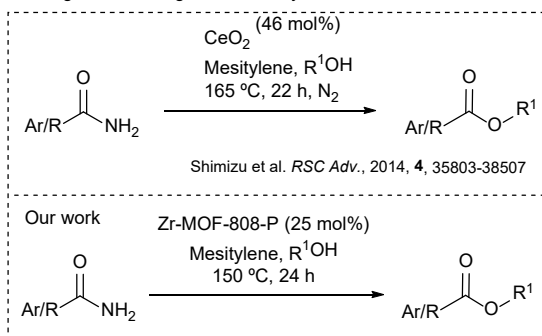
Scheme 1. Representative examples using homogeneous and heterogeneous methodologies for the amide esterification.

Transition metals have been employed as catalysts in esterification reactions. Garg's group has demonstrated the amide activation with a nickel catalyst by an oxidative addition mechanism (**Scheme 1**).[23,24,25,26] Inorganic salts containing Cu (II) have been explored for the activation of amides, where the transition metal coordinates the nitrogen atom inducing a significant distortion in the structure. Bannwarth *et al.* gave a practical approach to this strategy, performing a methodology for the protection and deprotection of aromatic carboxylic acids through *N,N*-bis(2-picolyl)amide systems.[27,28,29]

In the last decade, a few examples of the amide esterification catalyzed by heterogeneous catalysts have been reported. In 2014, the role of cerium oxide as heterogeneous catalyst in the amide esterification was described.[30,31] Shimizu *et al.* provided a strategy for the amide alcoholysis employing CeO_2 at 165 °C under inert atmosphere (**Scheme 1**). The authors proposed that the synergy between Lewis acid and base sites on CeO_2 surface favors the activation of the amide group. The esterification reaction mechanism catalyzed by CeO_2 has been demonstrated by density functional theory calculations, *in situ* FT-IR spectroscopy and catalytic studies. We will show later the much higher activity and selectivity for amide esterification of the Zr-MOF-808 proposed here.

Metal-organic frameworks (MOFs) are a class of materials built from metallic clusters and organic linkers via coordination bonds.[32] The most attractive features of MOFs are their intrinsic properties, such as crystalline nature, high porosity, stability and surface area.[33,34] MOF-based materials have been found to be suitable catalysts to produce certain products with high industrial value due to their functional active sites along with the potential inner porosity that allows guest molecules to access the pores.[35,36,37] MOFs show high versatility thanks to the ability of modifying the organic linker and metal node, which offers a fine-tune control of the pore size or their inherent Lewis acidity, allowing the design of more selective processes.[38,39,40,41,42]

Recently, HKUST-1 (Cu (II)) has shown a mimetic activity of trypsin enzyme for the hydrolysis of bovine serum and casein albumin.[43] However, this solid is moisture sensitive, presenting a limited stability. Zirconium- and hafnium-based MOFs have demonstrated a remarkably better stability and robustness, compared with MOFs presenting other transition metals.[44] Indeed, the activity and stability of these MOFs have been demonstrated even in the presence of water and organic acids.[45,46,47,48] Interestingly, Zr-MOF-808 has been used as an effective heterogeneous catalyst for the peptide bond hydrolysis of a series of dipeptides.[49] The reaction mechanism involves the interaction of the amino acid terminal groups with the MOF ligands to activate the amide bond.

Based on our preliminary research,[45,46] we propose the use of MOFs containing group 4 metals (zirconium and hafnium) as artificial enzyme-type materials for the amide esterification reaction, since they present the adequate confined spaces and active sites to undergo this target reaction (**Scheme 1**). These solids have been exhaustively characterized, with emphasis on determining their active sites. Furthermore, a wide scope of esterification reactions with different functionalized amides and alcohols has been
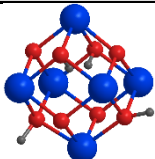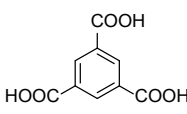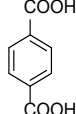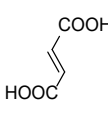
studied. A mechanism for the amide esterification reaction has been proposed based on kinetic models and *in situ* FT-IR studies.

Results and Discussion

Zr - based MOFs as catalysts for amide esterification

Previous studies have described the utilization of various MOFs as heterogeneous catalysts for the amide hydrolysis.[43,49] However, it's the first time that MOFs are used as catalysts for amide esterification. Our attention has been focused in different zirconium- and hafnium-based MOFs for catalytic amide esterification due to their potential physico-chemical properties. Zr-MOF-808, with the nominal chemical formula $Zr_6(\mu^3\text{-}O)_4(\mu^3\text{-}OH)_4\text{-}(BTC)_2(HCOO)_6$, was described for the first time in 2014.[50] Each metallic cluster is 6-connected in a spn topology and its framework generates tetrahedral and adamantane-like cages (4.8 and 18.4 Å, respectively **Table 1**). Zr-MOF-808-P[51] has been prepared following recently reported adapted procedure, using 3 equivalents of $ZrCl_4$ per each equivalent of organic linker (1,3,5-benzenetricarboxylic acid, H_3BTC) to increase potential active sites, while Zr-MOF-808 has been synthesized from 1 equivalent of $ZrCl_4$ per each equivalent of organic linker. Isoreticular Hf-MOF-808[44] has been prepared here using $HfCl_4$, as metal source.

Table 1. Structural characteristics of different MOFs and their metallic clusters

	Metal cluster		
Metal cluster			Color code. Blue: metal; Red: oxygen; Grey: hydrogen
	MOF-808	UiO-66	MOF-801
Formula	$M_6O_4(OH)_4$ $(BTC)_2(HCOO)_6$	$M_6O_4(OH)_4$ $(BDC)_6$	$M_6O_4(OH)_4$ $(FA)_6$
Ligand			
Connectivity	6-connected	12-connected	12-connected
Pore size (Zr-MOF)	4.8 and 18.4 Å	8.4 and 11 Å	5.6 and 7.4 Å

Besides MOF-808, we have also evaluated other MOF structures, such as UiO-66[52] and MOF-801.[53] Zr-UiO-66 consists of a 12-connected (1,4-benzenedicarboxylate, BDC) zirconium cluster while Zr-MOF-801 contains twelve fumaric linkers (FA). Both MOF structures have a fcu topology with tetrahedral and octahedral cages (8.4 and 11 Å for Zr-UiO-66 and 5.6 and 7.4 Å for Zr-MOF-801, **Table 1**). Considering this, their confined space will be smaller than in the case of Zr-MOF-808. These materials were prepared using a similar synthetic procedure to anticipate a similar degree of defects in their frameworks.

FULL PAPER

All these prepared materials have been characterized and the obtained data correlate well with the characterization reported previously in the literature. In general, the solids have shown high surface area, crystallinity and excellent thermal stability (See Supporting Information, section 2.1 and 2.2).

The prepared zirconium- and hafnium-based MOFs were tested in the esterification reaction of benzamide with n-butanol, using 25 mol% metal loading at 150 °C. The reaction was followed over time by gas chromatography. The highest activity was observed for Zr-MOF-808-P (**Figure 1**), fact that could be expected due to the lower connectivity within the structure (**Table 1**).
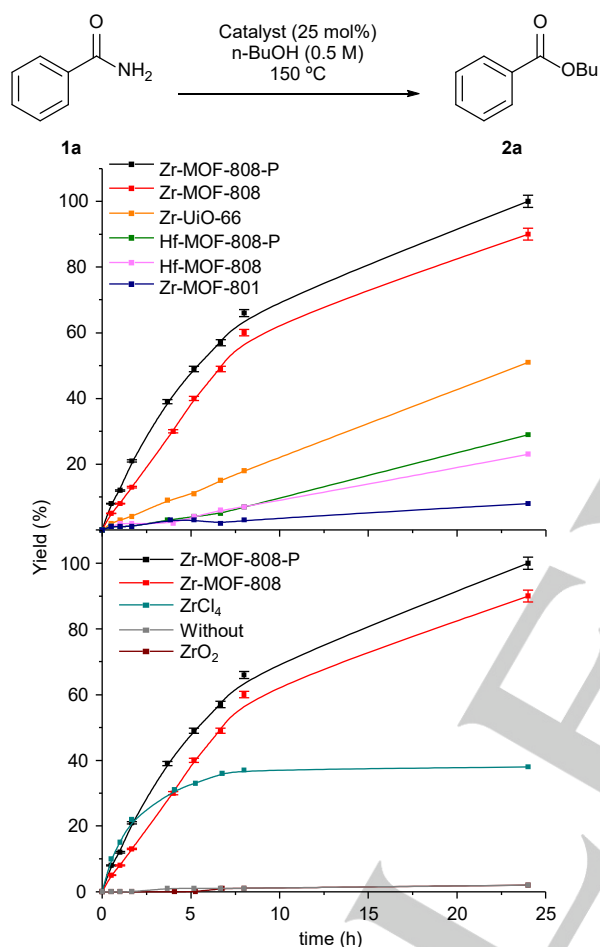

Figure 1. Kinetic study of the solvolysis of benzamide with n-butanol with several catalysts. Reaction conditions: Amide **1a** (0.3 mmol), catalyst (0.075 mmol, 25 mol%), n-butanol (0.6 ml, 0.5 M), 150 °C, n-dodecane (0.05 mmol) as external standard.

The calculated initial rate when using Zr-MOF-808-P was 62.0 mM/h (**Table 2. Entry 1**), which was 1.7 times higher compared with Zr-MOF-808 (**Table 2. Entry 2**). This difference in activity could be attributed to the lower number of active sites in the Zr-MOF-808 that shows lower degree of linker defects (as it will be discussed in the next section). In the case of Hf-MOF-808-P, the reaction rate decreased notably up to 4.2 mM/h (**Table 2. Entry 3**). The lower activity could be explained by the different acid-base properties of the metal clusters. The impact of the framework in the benzamide esterification with Zr-UiO-66 and Zr-MOF-801 as catalysts was also studied. The initial rates when using these catalysts were 10.7 and 2.2 mM/h, (**Table 2. Entry 5 and 7**) respectively (versus 62.0 mM/h for Zr-MOF-808-P). The

remarkable lower initial rates achieved with these materials compared to Zr-MOF-808-P could be attributed to the higher connectivity at the Zr clusters of the formers along with their smaller cages, fact that would mostly prevent the diffusion and stabilization of the reactants. In line with this, it should be noted that a higher meso/microporous ratio is observed in Zr-MOF-801 versus Zr-MOF-808. In view of the poor catalytic activity of the former, cluster connectivity appears decisive for the catalytic performance. The related Hf-based MOFs exhibit lower activity compared to the Zr counterparts (**Table 2. Entries 4, 6 and 8 versus Entries 2, 5, and 7**) once again attributed to the differences in the acid-base properties of the metal cluster. Then, it was accounted that Zr-MOF-808 has an adequate equilibrium between confined space and acid-base properties to promote the reaction. Regarding this, further details are shown below with the analysis of the acidic active sites in these MOFs by means of FT-IR spectroscopy using CO as probe molecule together with a mechanistic study by *in situ* FT-IR spectroscopy.

For a comparative purpose, the sub-units $ZrCl_4$ (metallic precursor), ZrO_2 and Zr_6-benzoate were employed in the reaction as catalysts (**Table 2. Entry 9, 10 and 11,** respectively). The initial reaction rate obtained with the inorganic precursor $Zrcl_4$ was comparable to that of Zr-MOF-808-P, but the reaction stopped after reaching 40 % yield, which indicates catalyst deactivation. In the case of ZrO_2, the activity is considerably lower compared to the rest of materials. Zr_6-benzoate shows a similar molecular cluster to Zr-MOF-808, however, the attained yield was 43 %.

Zr-MOF-808-P was also tested at lower loading (10 mol%) affording in this case 35 % yield of the desired product under identical reaction conditions (data not shown) pointing to the convenience of using 25 mol% loading to achieve high yields in reasonable reaction times.

Table 2. Solvolysis of benzamide with n-BuOH with different catalysts.

	Catalyst	%C[a]	%Y[a]	TON	TOF (h⁻¹)	r₀ (mM/h)
1	Zr-MOF-808-P	100	99	4.0	0.496	62.0
2	Zr-MOF-808	91	90	3.5	0.299	37.4
3	Hf-MOF-808-P	49	29	1.5	0.034	4.2
4	Hf-MOF-808	28	23	0.9	0.029	3.5
5	Zr-UiO-66	55	51	2.1	0.086	10.7
6	Hf-UiO-66	48	26	1.0	0.031	3.9
7	Zr-MOF-801	35	8	0.3	0.013	2.2
8	Hf-MOF-801	16	2	1.0	0.007	0.5
9	ZrCl₄	64	38	1.5	0.513	64.1
10	ZrO₂	23	2	0.1	0.003	0.4
11	Zr₆-benzoate	46	43	1.74	0.079	n.d.
12	Without	18	2	0.1	0.003	0.3

Reaction conditions: Amide **1a** (0.3 mmol), catalyst (0.075 mmol, 25 mol%), n-butanol (0.6 ml, 0.5 M), 150 °C. [a] Conversion and yield (%) has been determined by gas chromatography, with n-dodecane as external standard at 24 h. TON = moles of product obtained /moles of catalyst (referred to metal content). TOF = initial rate/catalyst concentration (h⁻¹). r₀ (mM/h) = initial rate for product formation. n.d.=not determined.

To check the behaviour of Zr-MOF-808-P as heterogeneous catalyst, it was evaluated by hot filtration test. To do that, the catalyst was removed from the reaction mixture by hot filtration after 1.7 h of reaction time at 150 °C, when the product yield reached 14 %. The reaction, once the solid was removed, was allowed to proceed for 22 hours where the product yield was 19 % (**Figure 2**), observing a slight progress of the reaction. Leaching of active sites to the reaction medium was analysed by ICP. It was found 65 ppm of Zr in the post-reaction solution measured after a first use of the catalyst (at 22 hours when the product reached 99 %). While 85 ppm of Zr (average of two experiments) were measured in the hot filtration test experiment after 1.7 hours reaction time. With these data, we could infer that those leached zirconium species could account for the low catalytic activity observed in the hot filtration test.
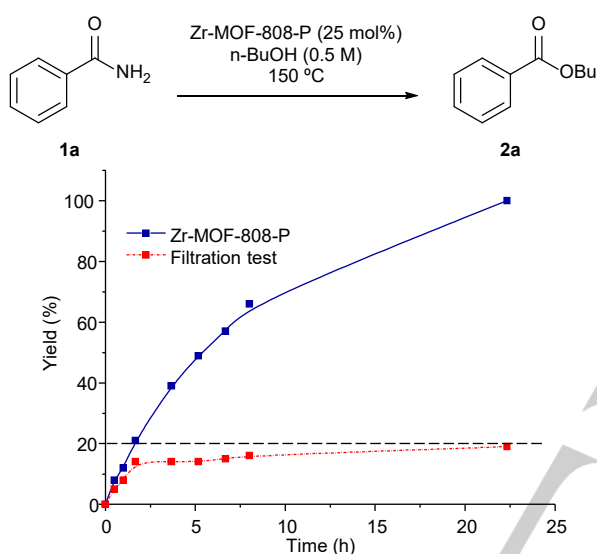

Figure 2. Kinetic study in the benzamide esterification catalyzed by Zr-MOF-808-P together with the hot filtering test. Reaction conditions: Benzamide **1a** (0.3 mmol), Zr-MOF-808-P (0.075 mmol, 25 mol%), n-butanol (0.6 ml, 0.5 M), 150 °C, n-dodecane (0.05 mmol) as external standard.
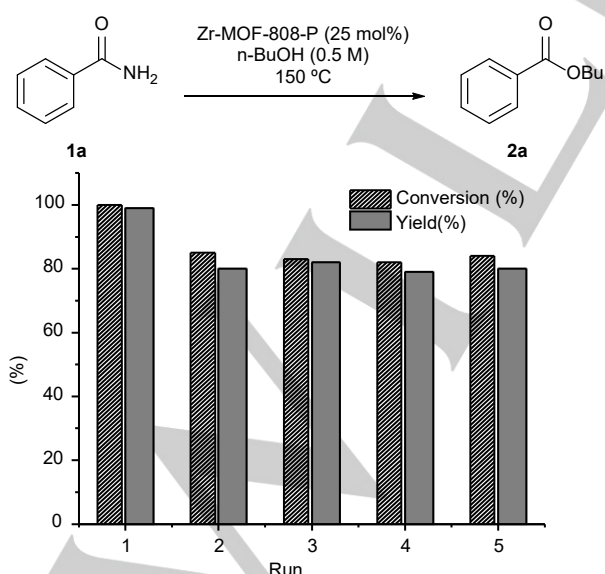

Figure 3. Evolution of conversion and yield of benzamide solvolysis in the reuse of the Zr-MOF-808-P catalyst.

The stability of the catalyst during the benzamide esterification was studied by successive reutilization finding that the catalyst could be reused for at least five consecutive cycles (**Figure 3**). After the first run, the yield decreased approximately 17 %, but it remained constant for further reuses. The recovered Zr-MOF-808-P was characterized by PXRD,^{13}C-CP MAS NMR, ICP and EA, FESEM, FT-IR, thermogravimetric analysis and N_2 physisorption isotherms (see Supporting information, section 2.3). ^{13}C-CP MAS NMR shows that, after the first use, the solid catalyst has experienced the exchange of the more labile non-structural formate linkers with benzoate ligands (Figure S24). Benzoic acid would be formed as a result of benzamide or butylbenzoate hydrolysis. Further, that exchange could be facilitated by the polar solvent (n-BuOH) employed in the reaction, as has been reported previously por Zr-MOF-808 when using methanol.[54] That structural change is also observed in the PXRD data measured in the five-times-used catalyst, showing differences in signal intensities and increased FWHM compared to the fresh Zr-MOF-808-P. In addition, the FESEM images after the first run indicate slight changes in the morphology with the appearance of a small amount of amorphous phase (see Supporting information, section 2.3). A reduction in the total pore volume was determined from the N_2 adsorption and desorption isotherm measured in the five-times-used catalyst. Those facts could account for the diminished catalytic activity observed after the first use of the catalyst. Nonetheless, the activity of the resulting catalyst was good in successive runs allowing product formation in 80% yield.

Such observed ligand exchange was also studied when using an aliphatic amide (butyramide) as starting material. In a similar manner, ^{13}C-CP MAS NMR spectrum (Figure S25) of the recovered Zr-MOF-808-P shows the presence of butyrate linker in place of formate accounting for ligand exchange during the reaction progress.

Scope of the amide esterification reaction

Since Zr-MOF-808-P exhibited remarkable activity toward amide esterification, a wide range of substrates has been investigated to demonstrate the general applicability of this catalytic system. The scope has been expanded to various primary aromatic amides substituted with different electron-donating groups on the ring, such as methyl (**3b, 3c**) or methoxy group (**3k**, **Figure 4**), and also with electron-withdrawing groups, such as trifluoromethyl (**3i**), nitro (**3h**) or halogens (**3d, 3e, 3f, Figure 4**), giving in all cases the desired products with high yields. It should be noted here that substrates bearing bromide and even iodide groups were well tolerated for which, in contrast, homogeneous transition-metal catalytic systems could not be applied due to extensive dehalogenation. Substituents in ortho positions are allowed although in these cases the corresponding esters are obtained in moderate yield probably due to steric hindrance (**2c, 2e, Figure 4**). With heteroaromatic amides, the performance of this methodology was good (around 70-100 % yield, **2l, 2m, Figure 4**). Also, aliphatic amides were examined obtaining high yields (**2p, 2q, 2t, Figure 4**), albeit the performance decreases slightly with the ramification in the alpha position on the chain (**2r, 2s, Figure 4**). As conclusion, this methodology could therefore be extended to a variety of functionalized amides.

Zr-MOF-808-P (25 mol%)
n-BuOH (0.5 M)
150 °C

R—C(=O)—NH₂ (1a, 3) → R—C(=O)—OBu (2)

2a, t = 24 h (36 h)
C^b = 100 %
Y^{a,b} = 99 % (92 %)

2b, t = 24 h (42 h)
C^b = 86 %
Y^{a,b} = 86 % (86 %)

2c, t = 48 h
C^b = 50 %
Y^{a,b} = 39 %

2d, t = 24 h
C^b = 98 %
Y^{a,b} = 84 %

2e, t = 48 h
C^b = 64 %
Y^{a,b} = 53 %

2f, t = 24 h (42 h)
C^b = 90 %
Y^{a,b} = 74 % (90 %)

2g, t = 72 h
C^b = 31 %
Y^{a,b} = 15 %

2h, t = 24 h (42 h)
C^b = 97 %
Y^{a,b} = 93 % (87 %)

2i, t = 75 h
C^b = 100 %
Y^{a,b} = 87 %

2j, t = 75 h
C^b = 100 %
Y^{a,b} = 98 %

2k, t = 88 h (96 h)
C^b = 86 %
Y^{a,b} = 86 % (93 %)

2l, t = 24 h
C^b = 90 %
Y^{a,b} = 97 %

2m, t = 24 h
C^b = 84 %
Y^{a,b} = 71 %

2n, t = 72 h
C^b = 96 %
Y^{a,b} = 90 %

2o, t = 24 h (44 h)
C^b = 100 %
Y^{a,b} = 96 % (90 %)

2p, t = 24 h
C^b = 100 %
Y^{a,b} = 99 %

2q, t = 24 h
C^b = 100 %
Y^{a,b} = 95 %

2r, t = 24 h
C^b = 95 %
Y^{a,b} = 87 %

2s, t = 24 h
C^b = 78 %
Y^{a,b} = 81 %

2t, t = 24 h (44 h)
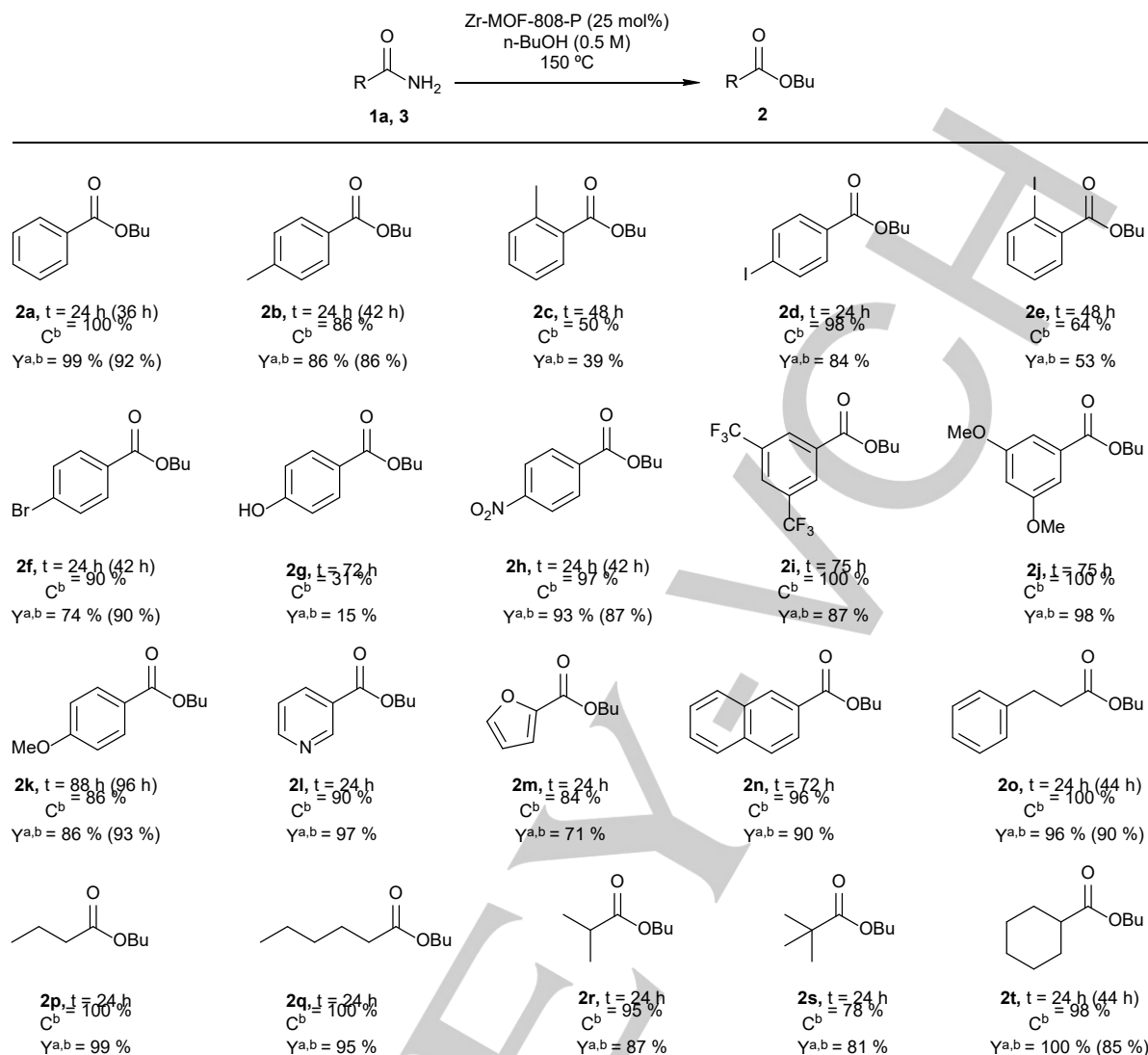C^b = 98 %
Y^{a,b} = 100 % (85 %)

Figure 4. Evolution of conversion and yield of benzamide solvolysis in the reuse of the Zr-MOF-808-P catalyst. Scope for solvolysis of amides with n-BuOH catalyzed by Zr-MOF-808-P. Reactions conditions: Amide **1a** or **3** (0.1 mmol), Zr-MOF-808-P (25 mol%), n-butanol (0.2 ml, 0.5 M), 150 °C. ^{a}In brackets, the yield of the product isolated by flash chromatography (1 mmol scale). ^{b}Conversion and yield (%) determined by ^{1}H NMR using 1,3,5- trimethoxybenzene as external standard.

Zr-MOF-808-P (25 mol%)
R'-OH (0.5 M)
150 °C, 24 h

1a → **2a, 4**

Ph—C(=O)—O-Bu
2a
C^a = 100 %
Y^a = 92 %

Ph—C(=O)—O-Hex
4b
C^a = 92 %
Y^a = 85 %

Ph—C(=O)—O-Oct
4c
C^a = 92 %
Y^a = 90 %

Ph—C(=O)—O-(sec-Pen)
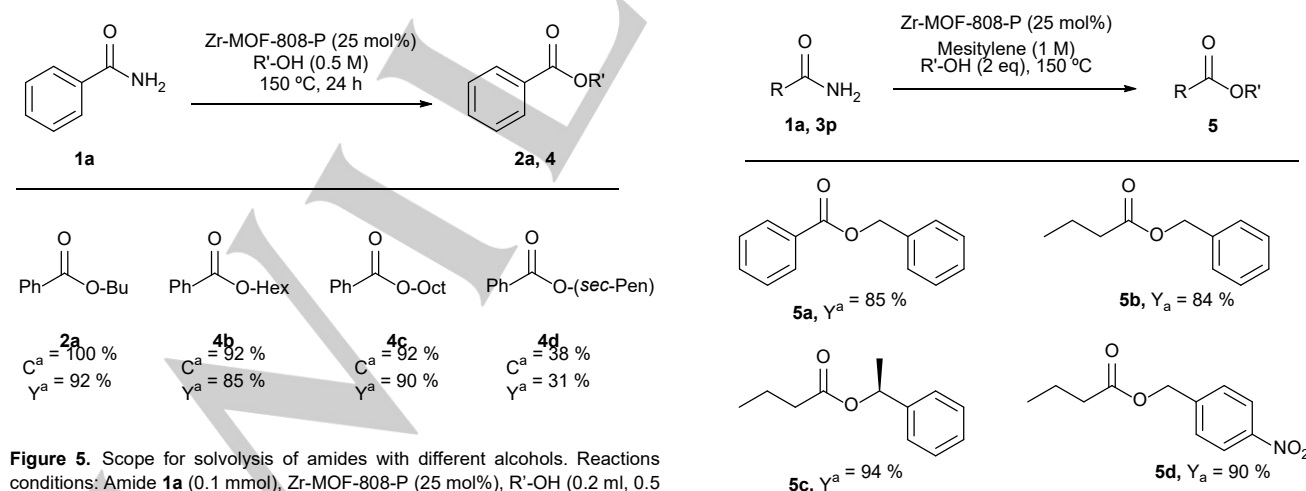**4d**
C^a = 38 %
Y^a = 31 %

Figure 5. Scope for solvolysis of amides with different alcohols. Reactions conditions: Amide **1a** (0.1 mmol), Zr-MOF-808-P (25 mol%), R'-OH (0.2 ml, 0.5 M), 150 °C, 24 h. ^{a}Conversion and yield (%) determined by ^{1}H NMR using 1,3,5-trimethoxybenzene as external standard.

Zr-MOF-808-P (25 mol%)
Mesitylene (1 M)
R'-OH (2 eq), 150 °C

R—C(=O)—NH₂ (1a, 3p) → R—C(=O)—OR' (5)

5a, Y$_a$ = 85 %

5b, Y$_a$ = 84 %

5c, Y$_a$ = 94 %

5d, Y$_a$ = 90 %

Figure 6. Extension of the methodology to the esterification of amides with alcohols in mesitylene. Reactions conditions: Amide **1a** or **3p** (1 mmol), Zr-MOF-808-P (25 mol%), R'-OH (2 mmol, 2 eq), mesitylene (1 ml, 1 M), 150 °C, 44 h. ^{a}Yield (%) of the product isolated by flash chromatography.
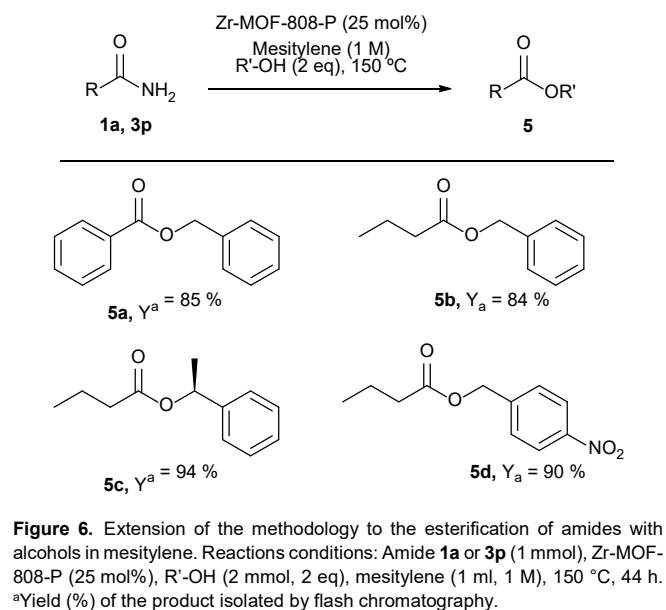
The alcohol scope was also considered in the benzamide esterification. Various alcohols with larger chains than n-butanol (such as n-hexanol and n-octanol) were tested in solvolitic conditions, obtaining in all cases good conversions and yields. A secondary alcohol, 2-pentanol, was also tested, achieving low yield in this case. (**Figure 5**).

Moreover, more complex alcohols, such as benzyl alcohol, *(S)*-1-phenylethanol or 4-nitrobenzyl alcohol, have been tested for benzamide esterification in non-solvolitic conditions, with only two equivalents of alcohol in mesitylene at 150 °C (**Figure 6**). In all cases, the product yields achieved were also excellent, approaching ~90 % for the different alcohols.
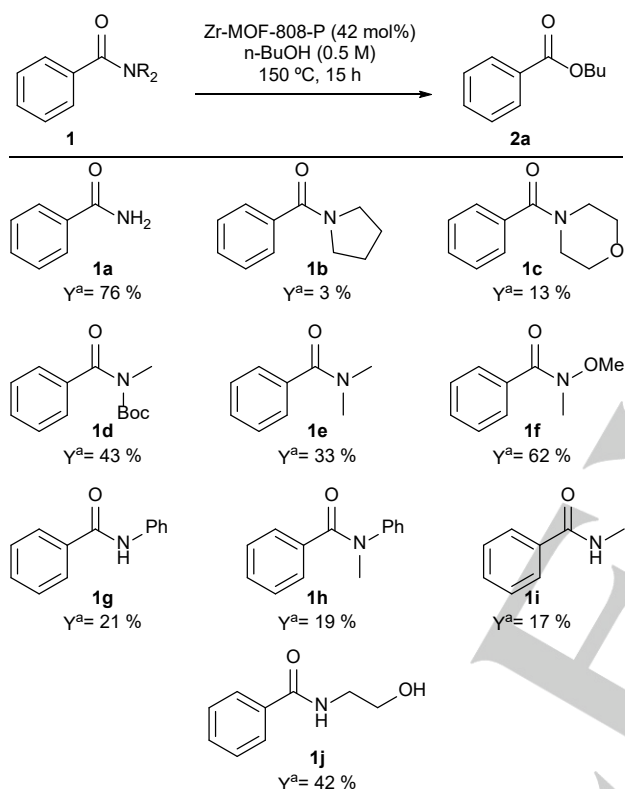
Figure 7. Selection of the appropriate leaving group in the amide structure with n-butanol catalyzed by Zr-MOF-808-P. Reactions conditions: Amide **1** (0.1 mmol), Zr-MOF-808-P (42 mol%), n-butanol (0.2 ml, 0.5 M), 150 °C, 15 h. [a]Yield (%) determined by gas chromatography, using n-dodecane (0.1 mmol) as external standard.

On the other hand, the nature of the leaving groups could be a determinant factor for reaction viability with amides, as it has been proposed in different literature reports.[20,55] As a proof of concept, a wide range of amides with different leaving group (non-activated, twisted and distorsioned amides) has been selected to study their esterification reaction using Zr-MOF-808-P as catalyst. Primary amides (**1a**) were efficiently converted to butyl benzoate (**2a**) (**Figure 7**).

This methodology could also be applied to a variety of amides, such as *N*-Boc-*N*-methylbenzamide, *N,N*-dimethylbenzamide, *N*-methoxy-*N*-methylbenzamide or *N*-(2-hydroxyethyl)benzamide (with an alternative mechanism *via* N,O-rearrangement)[18,19] (**1d, 1e, 1f, 1j, Figure 7**), with moderated conversion. Further, during the reaction, the thermal deprotection of *N*-Boc-

N-methylbenzamide generating *N*-methylbenzamide happened. So, butyl benzoate was obtained from these two amides. For *N*-benzoylpyrrolidine or *N*-benzoylmorpholine (**1b, 1c, Figure 7**), the transformation was less successful. In the case of compounds **1g** and **1h**, it was observed that the released amines (anilines) form by-products (*N*-butylanilines) as a result of the *N*-alkylation reaction with the solvent n-butanol.

Role of acid sites in MOFs catalytic performance

Thermodynamically, in some case, the number of defects in the material structure is related to its stability.[56,57] In MOFs, which are crystalline solids in all their infinite network, these defects could be introduced spontaneously or in a controlled manner, modulating their final properties.[58,52] Active sites are coordinatively unsaturated metal centres (CUS) present in the MOF intrinsically by design and additionally as a consequence of defects derived from uncoordinated ligands to the metal centre. This means that there is a direct relation between defects and active sites.

Amide esterification can be catalyzed by acid sites (Brönsted and Lewis)[14,22,27,29] and by catalysts containing both acid and base centres.[59,19,30] Then, to identify the acidity of active sites in these MOFs, they were exposed to CO as probe molecule and analysed by FT-IR spectroscopy. CO has a weak basicity to be able to discriminate between Brönsted and Lewis acid sites.[60,61,62] With a pre-treatment of both Zr-MOF-808 samples at 100 °C under high-vacuum (**Figure 8. a** and **b**), two bands (2153 and 2147 cm^{-1}) can be observed after deconvolution. At the same time, a band at 3675 cm^{-1} disappears in favour of the appearance of another (3606 cm^{-1}). This fact evidences the presence of two different Brönsted acid sites, associated with μ^3-OH group of metal cluster.[63,58] We also observe a band at 2138 cm^{-1} related to physisorbed CO.[61,62]

Moreover, when these samples were pre-treated at 250 °C under high-vacuum (**Figure 8. c** and **d**) for release of formate linkers[54] and/or dehydroxylation of the cluster,[56] two bands are identified at 2155 cm^{-1}, corresponding to the interaction of CO with Brönsted acid sites, and at 2177 cm^{-1}, being assigned to Lewis acid centres. This means that one of the types of Brönsted acid sites was lost with the dehydroxylation, generating Lewis acid sites.
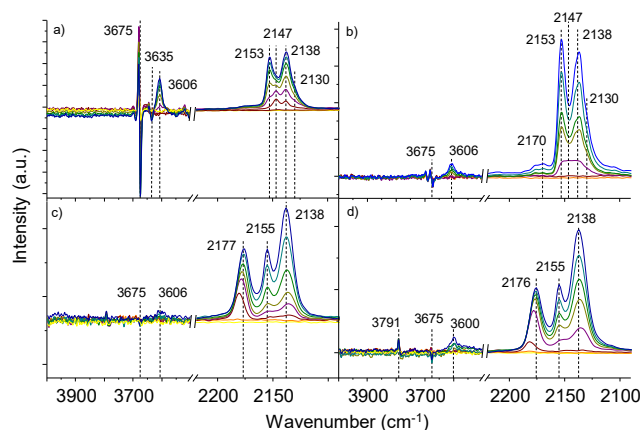

Figure 8. Difference FT-IR spectra for CO adsorption of a) Zr-MOF-808-P and b) Zr-MOF-808 pre-treated at 100 °C; c) Zr-MOF-808-P and d) Zr-MOF-808 pre-treated at 250 °C.

Then, Hf-MOF-808-P (with a pre-treatment at 250 ºC) was studied (see SI, Section 2.2.3). For Hf-MOF-808-P, the relative intensity of the signals centered at 2171 and 2153 cm^{-1}, related to the Lewis and Brönsted acid sites respectively are lower than for Zr-MOF-808.

Finally, Zr-UiO-66 (with a pre-treatment at 200 ºC) was analysed. The Brönsted acid sites (at 2153 cm^{-1}) are the mostly presented in this sample (see SI, section 2.2.3).

On the hypothesis that the intensity in the CO adsorption is proportional to the concentration of acid sites, the integrals of the vibration signals can be directly correlated with the number of acid centres in the MOF.[61,62] Then, the two IR bands (2155 and 2177 cm^{-1}) at the maximum adsorption of CO for each MOF were deconvoluted. From these calculations, it can be concluded that Zr-MOF-808-P possesses a relative amount of acid centres slighty higher than Zr-MOF-808 for dehydroxylated formula (**Table 3**). Furthermore, the number of btc linkers was determined by TGA analysis[54] (see SI, section 2.2.2.) finding that Zr-MOF-808-P presents 1.7 linkers versus 1.9 btc linkers detected for Zr-MOF-808 revealing a higher degree of defects for the Zr-MOF-808-P framework.

Table 3. Relative amount of Lewis and Brönsted acid centres (a. u,) at the maximum adsorption of CO (with a pre-treatment at 250 °C).

Acid	v (cm^{-1})	Zr-MOF-808-P	Zr-MOF-808
Lewis	2176	0.70	0.68
Brönsted	2155	0.50	0.47

With regards to Hf-MOF-808-P and Zr-UiO-66 samples, a relative lower amount of acidic centers than for Zr-MOF-808 materials was determined (see SI, Table S3). This is in line with the diminished catalytic performance of the former solids.
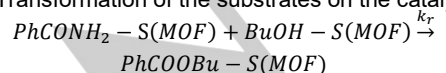
Kinetic study of the esterification of benzamide with n-butanol catalyzed by Zr-MOF-808-P

We have studied the kinetics of the benzamide esterification with n-butanol, and a Langmuir-Hinshelwood-Hougen-Watson (LHHW)[64] type kinetic model has been proposed to explain the mechanism for this reaction. This model considers that there is only one type of active site on the catalyst surface, on which substrates can be adsorbed. On those bases, the reaction mechanism would be as follows:
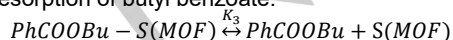
- Adsorption of the benzamide and n-butanol on MOF.

$$PhCONH_2 + S(MOF) \overset{K_1}{\leftrightarrow} PhCONH_2 - S(MOF)$$
$$BuOH + S(MOF) \overset{K_2}{\leftrightarrow} BuOH - S(MOF)$$
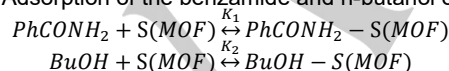
- Transformation of the substrates on the catalyst.

$$PhCONH_2 - S(MOF) + BuOH - S(MOF) \overset{k_r}{\rightarrow}$$
$$PhCOOBu - S(MOF)$$

- Desorption of butyl benzoate.

$$PhCOOBu - S(MOF) \overset{K_3}{\leftrightarrow} PhCOOBu + S(MOF)$$

Then, it is considered that the surface reaction is the rate-controlling step and the adsorption and desorption processes are in equilibrium. Thus, the rate equation can be formulated as follows:

$$r_{PhCOOBu} = K_{het} \left(\frac{[PhCONH_2][BuOH]}{(1 + K_1[PhCONH_2] + K_2[BuOH] + K_3[PhCOOBu])^2} \right)$$

The kinetic equation was solved with the initial rate method. The initial rate was analysed considering three variables (amount of benzamide, n-butanol or butyl benzoate) and maintaining the other parameters constant (see SI, section 3.3). The linearization for each case offered an equations system, where the adsorption constants could be calculated (see Supporting Information, section 3.3). This adsorption constants are K_1 (PhCONH$_2$) = 8.53, K_2 (BuOH) = 0.95 and K_3 (PhCOOBu)= 24.17. n-BuOH was weakly adsorbed on the MOF-808-P surface, explaining the need for a higher amount of n-BuOH in the reaction media, and that butyl benzoate was adsorbed more strongly than benzamide. The knowledge acquired from the kinetic study has been very useful to design the *in situ* FT-IR experiments, which will be studied in the next section, when discussing the molecular reaction mechanism.

Mechanistic studies by *in situ* FT-IR

The possible reaction mechanism for benzamide esterification with n-butanol catalyzed by Zr-MOF-808-P has been investigated by *in situ* FT-IR spectroscopy. Firstly, the interaction of benzamide with the potential active sites has been studied. **Figure 9** shows the FT-IR spectra of a) Zr-MOF-808-P and b) Zr-MOF-808-P with pre-adsorbed benzamide. After the addition of benzamide, a splitting in the band at 3677 cm^{-1} together with an increment of the signal centered at 3300 cm^{-1} was observed, which could be attributed to the interaction between benzamide and the hydroxyl groups of metal cluster via intermolecular hydrogen bonding. The bands associated with carbonyl group (~1600 cm^{-1}) of benzamide, which would be of high utility, cannot be observed because they fall within the metal-organic framework region. Based on the higher zirconium oxophilicity, we propose that the most likely interaction between the Zr cluster and benzamide can occur via Brönsted-Lewis acid pair and the benzamide molecule, through the carbonyl group (Zr(MOF)···O=C(benzamide)) and the NH$_2$ group (O-H(MOF)···N-H$_2$(benzamide)) (**Figure 9**).[65]
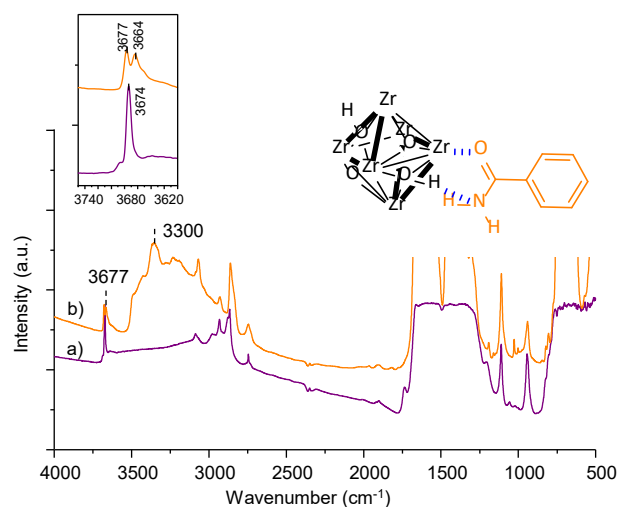

Figure 9. FT-IR spectra of a) Zr-MOF-808-P and b) Zr-MOF-808-P with pre-adsorbed benzamide.

FULL PAPER

Subsequently, n-BuOH was dosed on Zr-MOF-808-P with pre-adsorbed benzamide at room temperature. Two new signals appeared at 1070 and 1030 cm^{-1} related to C-O stretching vibration bands of n-BuOH due to the formation of Lewis pair Zr(MOF)···O-H(n-BuOH) in the terminal and bridging node, respectively[66] (**Figure 10**). Furthermore, the signal at 3674 cm^{-1} associated with hydroxyl groups of metal cluster disappeared in favour of the increment of a new band centered at 3000 cm^{-1} which can be attributed to the hydrogen bond interaction between O(MOF)···H-O(n-BuOH) (see Supplementary Information, section 3.4).

In a different set of experiments, the IR cell was then heated up from 50 to 100 and 150 °C sequentially, allowing the reaction for 45 minutes at each temperature. In the resulting FT-IR spectra (**Figure 10**), a decreasing in the signal centered at 1070 cm^{-1} together with the formation of a new band at 1146 cm^{-1} were observed. Further increment of the latter band is observed when the sample was heated up at 150 °C which may indicate formation of butoxide species, preferably in the terminal positions of metal cluster (**Scheme 3**).[67,68,66] These species are more active for a nucleophilic attack than n-butanol, favouring the amide esterification.

In a separate experiment, n-BuOH was dosed directly on Zr-MOF-808-P (without pre-adsorbed benzamide). In a similar manner, butoxide species formation was accounted upon sample heating to 150 ºC with the observation of the appearance of the band at 1146 cm^{-1} (see SI, section 3.4).

Sheme 3. Butoxide formation on Zr-MOF-808.

Based on the results of the *in situ* FT-IR study and related precedents,[69,66,31] a plausible reaction mechanism has been proposed (**Scheme 4**): (1) Benzamide interacts with Zr-MOF-808-P through both, the Lewis acid sites (by binding between the coordinately unsaturated zirconia centres and the amide carbonyl) and the Brönsted acid centres (by forming hydrogen bonds between the hydroxyl groups of the solid and the nitrogen of the amide) (Intermediate A). (2) n-Butanol is anchored to the Lewis acid centres by the oxygen atom. This coupling is reinforced by the interaction between the hydrogen of the alcohol and the basic O^{2-} centre of the Zr-MOF-808-P (Intermediate B). At 150 °C, butoxide formation is occurring (Intermediate C). (3) Butoxide intermediate reacts with the neighbouring benzamide to yield the product releasing NH$_3$. The final product, butyl benzoate, is desorbed liberating the active centre.
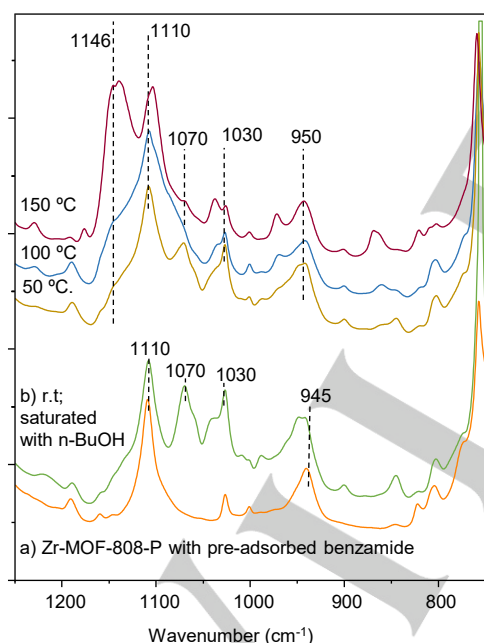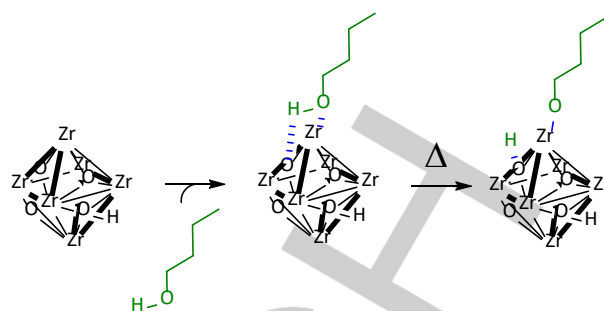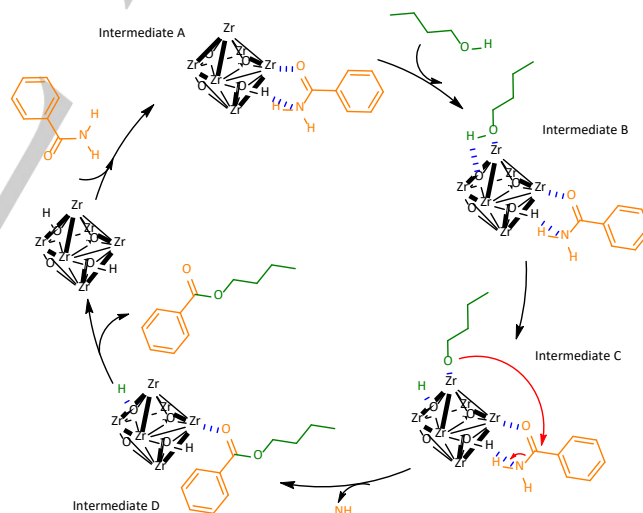

Figure 10. FT-IR spectra in 1250-750 cm^{-1} range of a) Zr-MOF-808-P with pre-absorbed benzamide b) Zr-MOF-808-P with pre-absorbed benzamide saturated with n-BuOH at room temperature. The temperature was increased for the latter sample at 50 °C, 100 °C and 150 °C and FT-IR spectra recorded and shown at the top of the graphic, respectively.

Scheme 4. Proposal mechanism for the benzamide esterification with n-BuOH catalyzed by Zr-MOF-808-P.

Conclusion

Zr-MOF-808-P, with hydrophobic pockets conferred by organic ligands and hydrophilic Zr clusters, presents specific confined spaces and active sites for amide esterification. More interestingly, compared to other homogeneous catalysts, Zr-MOF-808-P can activate primary, secondary and tertiary amides and presents a wide scope in aromatic

and aliphatic functionalised amides. Moreover, the esterification of amides is also feasible under non-solvolitic conditions. This material shows thermal stability acting as a heterogeneous catalyst, that can be recovered and reused for several reaction cycles. *In situ* FT-IR studies and kinetic modelling allow a better understanding of the reaction pathway at the molecular level. This material has the appropriated Brönsted-Lewis acid sites to activate both reacting substrates, the amide and the alcohol.

Experimental Section

MOF synthesis. Zr-MOF-808-P,[50] H₃BTC (1,3,5-benzenetricarboxylic acid) (0.52 g, 2.5 mmol) and ZrCl₄ (1.75 g, 7.5 mmol) were dissolved in a mixture of DMF/formic acid (226 ml, 1:1; 0.011 M) in a 500 ml flat bottom round flask, which was heated at reflux (120 °C) under magnetic stirring for four days. The precipitate was collected by vacuum filtration and washed three times with fresh DMF and subsequently three more times with fresh acetone. Then, the material was heated up at 110 °C under vacuum for two hours approximately. The final product was obtained as a white solid (0.52 g, 2.3 mmol, 92 % yield referred to ZrCl₄).

(For other MOFs, see SI, section 2.1.)

Esterification of amides. **General procedure of amide solvolysis**. Zr-MOF-808-P (0.25 mmol, 25 mol%), amide (1 mmol) and n-butanol (2 ml, 0.5 M) were added to a 10 ml pyrex glass tube. The reaction mixture was left to stir vigorously at 150 °C during the corresponding time. It was then filtered to separate the catalyst and washed thoroughly with ethyl acetate. The solvent was then removed in a rotavapor at reduced pressure and the reaction crude was purified by column flash chromatography using hexane/ethyl acetate as the eluent. All products obtained within this work have been described previously and characterization in the literature was used for comparison. **General procedure of amide esterification in mesitylene**. A reactive mixture was prepared with Zr-MOF-808-P (0.25 mmol, 25 mol%), the amide (1 mmol), the corresponding alcohol (2 mmol) and mesitylene (1 ml, 1 M)) as solvent in a 10 ml pyrex glass tube. It was shaken vigorously at 150°C for 44 h and then filtered to separate the catalyst, which was washed with ethyl acetate. The solvent was then removed in a reduced pressure rotary evaporator and the crude product was purified by column flash chromatography using hexane/ethyl acetate as the eluent. All products obtained within this work have been described previously and characterization in the literature was used for comparison.

(For other procedures about esterification of amides, see SI, section 3.2)

Acknowledgements

Keywords: Metal-organic frameworks • Amides • Heterogeneous catalysis • Kinetics • Reaction mechanisms

1   L. Pauling, *The Nature of the Chemical Bond*, Ithaca, NewYork, Third., 1960.

2   N. Sewald and H.-D. Jakubke, *Peptides: Chemistry and Biology*, Weinheim, Germany, Second., 2002.

3   V. Andrushko and N. Andrushko, *Stereoselective Synthesis of Drugs and Natural Products*, New Jersey, 2013.

4   A. Greenberg, C. M. Breneman and J. F. Liebman, *The Amide Linkage: Structural Significance in Chemistry, Biochemistry, and Materials Science*, Chichester, New York, 2000.

5   A. Radzicka and R. Wolfenden, *J. Am. Chem. Soc.*, 1996, **118**, 6105–6109.

6   R. A. R. Bryant and D. E. Hansen, *J. Am. Chem. Soc.*, 1996, **118**, 5498–5499.

7   R. M. Smith and D. E. Hansen, *J. Am. Chem. Soc.*, 1998, **120**, 8910–8913.

8   S. Weinreb and S. Nahm, *Tetrahedron Lett.*, 1981, **22**, 3815–3818.

9   A. J. Kiessling and C. K. McClure, *Synth. Commun.*, 1997, **27**, 923–937.

10 D. J. A. Schedler, A. G. Godfrey and B. Ganem, *Tetrahedron Lett.*, 1993, **34**, 5035–5038.

11 J. T. Spletstoser, J. M. White, A. R. Tunoori and G. I. Georg, *J. Am. Chem. Soc.*, 2007, **129**, 3408–3419.

12 E. H. White, *J. Am. Chem. Soc.*, 1955, 6011–6014.

13 R. F. Abdulla and R. S. Brinkmeyer, *Tetrahedron*, 1979, **35**, 1675–1735.

14 A. B. Charette and P. Chua, *Synlett*, 1998, 163–165.

15 G. Li, P. Lei and M. Szostak, *Org. Lett.*, 2018, **20**, 5622− 5625.

16 M. Petelin, Z. Pavlica, S. Bizimoska and M. Šentjurc, *Int. J. Pharm.*, 2004, **270**, 83–91.

17 M. Tamura, K.-I. Shimizu and A. Satsuma, *Chem. Lett.*, 2012, **41**, 1397–1405.

18 Y. Kita, Y. Nishii, T. Higuchi and K. Mashima, *Angew. Chemie - Int. Ed.*, 2012, **51**, 5723 –5726.

19 Y. Nishii, S. Akiyama, Y. Kita and K. Mashima, *Synlett*, 2015, **26**, 1831–1834.

20 C. Liu and M. Szostak, *Chem. A Eur. J.*, 2017, **23**, 7157–7173.

21 S. Adachi, N. Kumagai and M. Shibasaki, *Chem. Sci.*, 2017, **8**, 85–90.

22 H. Wu, W. Guo, S. Daniel, Y. Li, C. Liu and Z. Zeng, *Chem. A Eur. J.*, 2018, **24**, 3444–3447.

23 L. Hie, N. F. Fine Nathel, T. K. Shah, E. L. Baker, X. Hong, Y. F. Yang, P. Liu, K. N. Houk and N. K. Garg, *Nature*, 2015, **524**, 79–83.

24 J. E. Dander, N. A. Weires and N. K. Garg, *Org. Lett.*, 2016, **18**, 3934–3936.

25 N. A. Weires, E. L. Baker and N. K. Garg, *Nat. Chem.*, 2016, **8**, 75–79.

26 L. Hie, E. L. Baker, S. M. Anthony, J.-N. Desrosiers, C. Senanayake and N. K. Garg, *Angew. Chemie - Int. Ed.*, 2016, **55**, 15129–15132.

27 M. C. Bröhmer, S. Mundinger, S. Bräse and W. Bannwarth, *Angew. Chemie - Int. Ed.*, 2011, **50**, 6175 –6177.

28 S. Mundinger, U. Jakob and W. Bannwarth, *Chem. A Eur. J.*, 2014, **20**, 1258–1262.

29 S. Mundinger, U. Jakob, P. Bichovski and W. Bannwarth, *J. Org. Chem.*, 2012, **77**, 8968–8979.

30 S. M. A. H. Siddiki, A. S. Touchy, M. Tamura and K.-I. Shimizu, *RSC Adv.*, 2014, **4**, 35803–35807.

31 T. Kamachi, S. M. A. H. Siddiki, Y. Morita, M. N. Rashed, K. Kon, T.

Toyao, Shimizu, Ken-ichi and K. Yoshizawa, *Catal. Today*, 2018, **303**, 256–262.

32 Y. G. Sun, X. M. Yan, F. Ding, E. J. Gao, W. Z. Zhang and F. Verpoort, *Inorg. Chem. Commun.*, 2008, **11**, 1117–1120.

33 H. Deng, S. Grunder, K. E. Cordova, C. Valente, H. Furukawa, M. Hmadeh, F. Gándara, A. C. Whalley, Z. Liu, S. Asahina, H. Kazumori, M. O'Keeffe, O. Terasaki, J. F. Stoddart and O. M. Yaghi, *Science (80-.)*., 2012, **336**, 1018–1024.

34 O. K. Farha, I. Eryazici, N. C. Jeong, B. G. Hauser, C. E. Wilmer, A. A. Sarjeant, R. Q. Snurr, S. T. Nguyen, A. Ö. Yazaydin and J. T. Hupp, *J. Am. Chem. Soc.*, 2012, **134**, 15016–15021.

35 P. García-García, M. Müller and A. Corma, *Chem. Sci.*, 2014, **5**, 2979–3007.

36 Y. H. Vo, T. V. Le, H. D. Nguyen, T. A. To, H. Q. Ha, A. T. Nguyen, A. N. Q. Phan and N. T. S. Phan, *J. Ind. Eng. Chem.*, 2018, **64**, 107–115.

37 J. Baek, B. Rungtaweevoranit, X. Pei, M. Park, S. C. Fakra, Y.-S. Liu, S. A. Alshmimri, S. Alshehri, C. A. Trickett, G. A. Somorjai and O. M. Yaghi, *J. Am. Chem. Soc.*, 2018, **140**, 18208–18216.

38 P. García-García, J. M. Moreno, U. Díaz, M. Bruix and A. Corma, *Nat. Commun.*, 2016, **7**, 10835.

39 S. Rojas-Buzo, P. García-García and A. Corma, *ChemCatChem*, 2017, **9**, 997–1004.

40 M. Lammert, C. Glißmann and N. Stock, *Dalt. Trans.*, 2017, **46**, 2425–2429.

41 T. Islamoglu, D. Ray, P. Li, M. B. Majewski, I. Akpinar, X. Zhang, C. J. Cramer, L. Gagliardi and O. K. Farha, *Inorg. Chem.*, 2018, **57**, 13246–13251.

42 S. Ullah, U. Yunus, M. H. Bhatti, P. D. Southon, K. Iqbal and S. Zaidi, *ChemistrySelect*, 2018, **3**, 10434–10438.

43 B. Li, D. Chen, J. Wang, Z. Yan, L. Jiang, D. Duan, J. He, Z. Luo, J. Zhang and F. Yuan, *Sci. Rep.*, 2014, **4**, 39–43.

44 S. Yuan, J. Qin, C. T. Lollar and H.-C. Zhou, *ACS Cent. Sci.*, 2018, **4**, 440–450.

45 S. Rojas-Buzo, P. García-García and A. Corma, *Green Chem.*, 2018, **20**, 3081–3091.

46 S. Rojas-Buzo, P. García-García and A. Corma, *ChemSusChem*, 2018, **11**, 432–438.

47 H.-B. Luo, M. Wang, S.-X. Liu, C. Xue, Z.-F. Tian, Y. Zou and X.-M. Ren, *Inorg. Chem.*, 2017, **56**, 4169–4175.

48 H.-Q. Zheng, C.-Y. Liu, X.-Y. Zeng, J. Chen, J. Lu, R.-G. Lin, R. Cao, Z.-J. Lin and J.-W. Su, *Inorg. Chem.*, 2018, **57**, 9096–9104.

49 H. G. T. Ly, G. Fu, A. Kondinski, B. Bueken, D. De Vos and T. N. Parac-Vogt, *J. Am. Chem. Soc.*, 2018, **140**, 6325–6335.

50 H. Furukawa, F. Gándara, Y.-B. Zhang, J. Jiang, W. L. Queen, M. R. Hudson and O. M. Yaghi, *J. Am. Chem. Soc.*, 2014, **136**, 4369–4381.

51 J. Jiang, F. Gándara, Y.-B. Zhang, K. Na, O. M. Yaghi and W. G. Klemperer, *J. Am. Chem. Soc.*, 2014, **138**, 12844–12847.

52 G. C. Shearer, S. Chavan, S. Bordiga, S. Svelle, U. Olsbye and K. P. Lillerud, *Chem. Mater.*, 2016, **28**, 3749–3761.

53 G. Wißmann, A. Schaate, S. Lilienthal, I. Bremer, A. M. Schneider and P. Behrens, *Microporous Mesoporous Mater.*, 2012, **152**, 64–70.

54 C. Jia, F. G. Cirujano, B. Bueken, B. Claes, D. Jonckheere, K. M. Van Geem and D. De Vos, *ChemSusChem*, 2019, **101**, 1256–1266.

55 J. Aubé, *Angew. Chemie - Int. Ed.*, 2012, **51**, 3063–3065.

56 Y. Bai, Y. Dou, L. Xie, W. Rutledge, J. Li and H. Zhou, *Chem. Soc. Rev.*, 2016, **45**, 2327–2367.

57 T. Devic and C. Serre, *Chem. Soc. Rev.*, 2014, **43**, 6097–6115.

58 H.-H. Mautschke, F. Drache, I. Senkovska, S. Kaskel and F. X. Llabrés i Xamena, *Catal. Sci. Technol.*, 2018, **8**, 3610–3616.

59 Y. Bourne-Branchu, C. Gosmini and G. Danoun, *Chem. A Eur. J.*, 2017, **23**, 10043–10047.

60 C. Morterra, G. Cerrato and S. Di Ciero, *Appl. Surf. Sci.*, 1998, **126**, 107–128.

61 V. L. Sushkevich, A. Vimont, A. Travert and I. I. Ivanova, *J. Phys. Chem. C*, 2015, **119**, 17633–17639.

62 D. M. Driscoll, D. Troya, P. M. Usov, A. J. Maynes, A. J. Morris and J. R. Morris, *J. Phys. Chem. C*, 2018, **122**, 14582–14589.

63 W. Zhou, Z. Ma, S. Guo, M. Wang, J. Wang, M. Xia, L. Jia, B. Hou, D. Li and Y. Zhao, *Appl. Surf. Sci.*, 2018, **427**, 867–873.

64 Y. Liu, J. Liu, H. Yan, Z. Zhou and A. Zhou, *ACS Omega*, 2019, **4**, 19462–19468.

65 M. Yashiro, T. Takarada, S. Miyama and M. Komiyama, *J. Chem. Soc. Chem. Commun.*, 1994, **2**, 1757–1758.

66 K. Xuan, Y. Pu, F. Li, J. Luo, N. Zhao and F. Xiao, *Chinese J. Catal.*, 2019, **40**, 553–566.

67 K. T. Jung and A. T. Bell, *J. Catal.*, 2001, **204**, 339–341.

68 L. Chen, S. Wang, J. Zhou, Y. Shen, Y. Zhao and X. Ma, *RSC Adv.*, 2014, **4**, 30968–30975.

69 L. Desidery, S. Chaemcheun, M. Yusubov and F. Verpoort, *Catal. Commun.*, 2018, **104**, 82–85.

Entry for the Table of Contents
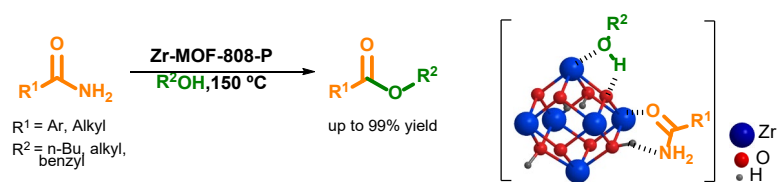
Zr-MOF-808-P is shown as an efficient reusable heterogeneous catalyst for amide esterification with ample substrate scope. Reaction mechanism is studied by *in situ* FTIR spectroscopy